Class. Quantum Grav. **13** (1996) A97–A106. Printed in the UK

Electrostatic charging of space-borne test bodies used in precision experiments

Y Jafry†, T J Sumner‡ and S Buchman§

† Space Science Department of ESA, ESTEC, Noordwijk, The Netherlands
‡ Astrophysics Group, Imperial College, London, UK
§ W W Hansen Experimental Physics Laboratory, Stanford University, Stanford, CA, USA

Abstract. Space-borne physics experiments involving the measurement of small motions of test bodies are likely to be limited by disturbance forces. Of particular concern are forces arising from electrostatic charging of the test body due to interactions with particle radiation. Estimates of charging rates have been computed using Monte Carlo particle-transport codes in combination with semi-empirical particle flux models. Results are presented for the STEP and LISA geometries, and are extrapolated for GP-B. The consequences of the charging are assessed for each experiment, and a method for alleviating the problem is discussed which uses the photoemission technique already in the hardware development phase for GP-B.

PACS number: 0480

1. Introduction

In addition to the usual concern of damage inflicted on sensitive electronic components, exposure to high-energy particle radiation can have direct adverse effects on ultra-sensitive experiments which rely on the measurement of the motion of test bodies. Cosmic rays, solar protons and geomagnetically trapped protons with energies in excess of ~ 100 MeV can penetrate the spacecraft structures, depositing energy (heat), momentum and electrical charge on the test bodies. Of these, charging is known to be the most significant [9]. Spurious forces can result from direct Coulomb interaction between the charged test body and surrounding conducting surfaces, and, for payloads without electromagnetic shielding, from Lorentz forces due to the motion of the charged bodies through the interplanetary magnetic field. Depending on the frequency spectra of these disturbances, they could limit the performance of the experiments.

Three candidate missions are investigated as examples: GP-B (Gravity Probe B) [1, 16] with four 24 g quartz spheres (gyroscopes) in a polar Earth-orbiting spacecraft at 650 km altitude; STEP (satellite test of the equivalence principle) [12] with multiple differential accelerometers (with 0.1 kg cylindrical test masses) in a polar Earth-orbiting spacecraft at 400 km altitude and LISA (laser interferometer space antenna) [6], which is a constellation of spacecraft in heliocentric orbits at 1 AU from the Sun, each containing a 1.2 kg gold–platinum cubic test body. In all cases the test bodies are mechanically isolated from their immediate surroundings.

0264-9381/96/SA0097+10$19.50

2. The particle radiation environment

2.1. Trapped protons and the South Atlantic Anomaly

The flux and energy spectrum of trapped particles encountered by a spacecraft depend on the orbital trajectory relative to the Earth's magnetic field. For low-altitude polar Earth orbits (GP-B and STEP), the spacecraft routinely pass through the South Atlantic Anomaly (SAA), a region where the intensity of trapped protons is elevated [10]. Figure 1 shows how the SAA proton energy spectra vary with orbit altitude, computed from the AP8 semi-empirical models [13, 17]. Since the spacecraft traverse the SAA every few orbits, there is a defined spectral signature in the disturbance. By contrast, for a purely equatorial orbit the spacecraft avoids the SAA and is free from trapped particles for altitudes below 500 km. Thereafter, the fluxes increase rapidly with altitude, reaching a maximum for an altitude of 5000 km, where the fluxes are orders of magnitude in excess of the SAA fluxes shown in figure 1.

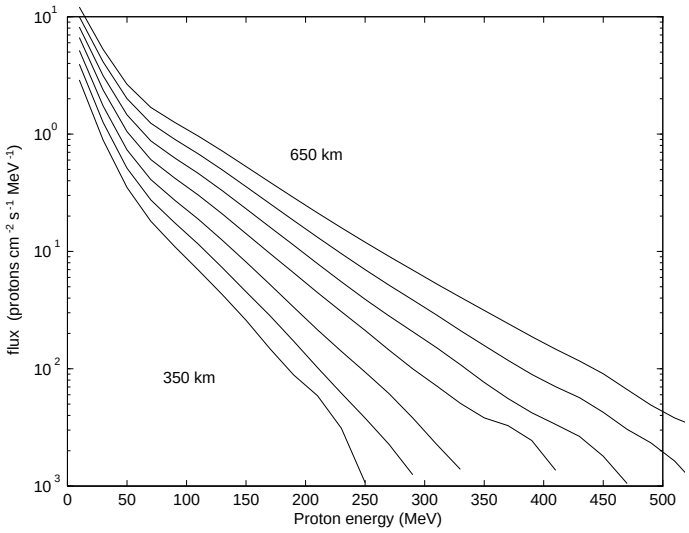

Figure 1. Orbit-averaged differential energy spectra for omnidirectional protons in the SAA. The curves cover the altitude range from 350 to 650 km, in steps of 50 km. The data correspond to the solar minimum, and are reduced by roughly a factor of two at the solar maximum (for energies in excess of 100 MeV).

2.2. Solar protons

An average solar flare event produces protons with an energy spectrum similar to those in the SAA, and lasts from a few hours to a few days. On rare occasions, anomalously large events occur, with fluxes many orders of magnitude higher. As discussed in [9], the frequency of flare events is skewed and asymmetric with respect to the solar cycle. In the seven-year neighbourhood of the solar maximum, about eight average flares per year can be expected. In the three-year neighbourhood of the solar minimum, the frequency drops to about one per year. An anomalously large event can occur at any time in the cycle.

2.3. Cosmic rays

Figure 2 shows spectra for the most abundant primary cosmic-ray constituents (protons and helium nuclei) inside the heliosphere. Although these primary fluxes are essentially isotropic, for Earth-orbiting spacecraft there will be a strong twice-per-orbit modulation due to latitude-dependent geomagnetic shielding (computed using the Störmer approximation [10]). The full extent of the flux will only be encountered near the geomagnetic poles, and will be strongly attenuated at lower latitudes, leading to a strong spectral signature in the disturbance.

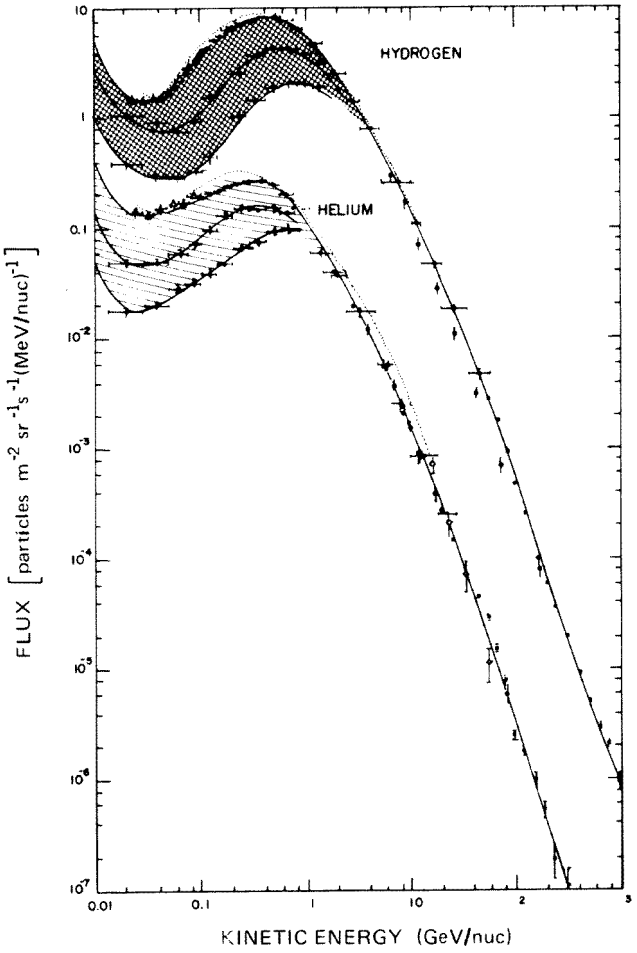

Figure 2. Cosmic ray differential energy spectrum (reproduced from [7]). The hydrogen spectrum has been multiplied by a factor of five to avoid clutter. For each species, the upper envelope indicates the solar minimum spectrum, the lower envelope indicates the solar maximum spectrum. The shaded area indicates the range of the solar modulation over a solar cycle.

3. Modelling the charge deposition

Charge deposition depends significantly on secondary particle generation and detailed geometry, both of which are difficult to model analytically. Consequently, the GEANT radiation transport code [5] has been used in this study. The code employs Monte Carlo particle ray-tracing techniques to follow all particles (incident and generated) through three-dimensional representations of a given geometry, taking into account all significant nuclear interactions. GEANT was used to determine the net charge deposited on the test bodies for a range of energies of isotropically incident particles striking the outer spacecraft walls. These were then convolved with semi-empirical models of fluxes for trapped particles [13, 17], solar protons [11] and cosmic rays [10] to determine the respective environmental charging rates.

Detailed discussion of the use of GEANT for analysing the STEP geometry can be found in [9]. Since that publication, the STEP model has been refined, and is summarized as follows. The two nested cylindrical test bodies—the inner plain cylindrical shell made from platinum, the outer 'belted' [12] cylindrical shell from silicon, both weighing 0.1 kg—are embedded in a quartz block, sized such that the outer mass is enveloped by 1 cm of quartz, which, in turn, is surrounded by a cubically symmetric tungsten shield (various thicknesses were investigated), enclosed in a cubically symmetric 2 cm thick aluminium box representing the combined spacecraft and cryostat structures.

The model constructed for LISA is summarized as follows. The 4 cm gold cubic test body is surrounded on all faces by 25 μm gold electrodes mounted on a cubically symmetric 15 mm shell of quartz, enclosed in a 5 mm thick titanium vacuum housing, surrounded by 1 cm of carbon-epoxy representing the spacecraft structure. On two opposing faces of the cube, quartz windows (7 mm diameter) have been inserted in the titanium, quartz and electrode layers, representing the access windows for LISA's laser beams.

GEANT is only valid for energies in excess of 10 keV. To check whether low-energy ($\leqslant 10$ keV) electrons not modelled by GEANT could significantly affect the charge deposition, the ITS Monte Carlo code [8] was used to analyse the transport of low-energy electrons in the near vicinity (1 μm) of surfaces. It was found that these only become significant at high incident particle energies (~ 5000 MeV) when the electrons are generated in large quantities. Since there are relatively few incident particles with such high energies, the ultimate effect of the low-energy electrons on the final charge was found to be negligible (less than a few per cent).

3.1. Computed charging rates

Figure 3 shows the computed net charging of the STEP outer test mass for each pass through the centre of the SAA, for a range of orbit altitudes and tungsten shield thicknesses (the charging for the inner test mass, not shown, is consistently lower due to the extra shielding provided by the outer mass). Also shown in the figure is the charge rate (per orbit) due to cosmic rays, taking into account the geomagnetic modulation. Although helium accounts for only 10% of the cosmic-ray incident flux, it is found to produce 30% of the charging, owing to the comparatively high numbers of secondaries generated. The charging is always positive, corresponding to the dominance of protons (primary and secondary) stopping in the test mass, confirming earlier GEANT predictions [9]. Contrary to naive expectation, it is seen that the tungsten shield only alleviates the SAA charging up to a certain thickness (~ 6 cm), after which the charging increases with thickness (then dips again later). The reason for this behaviour is the trade-off between the number of secondaries produced

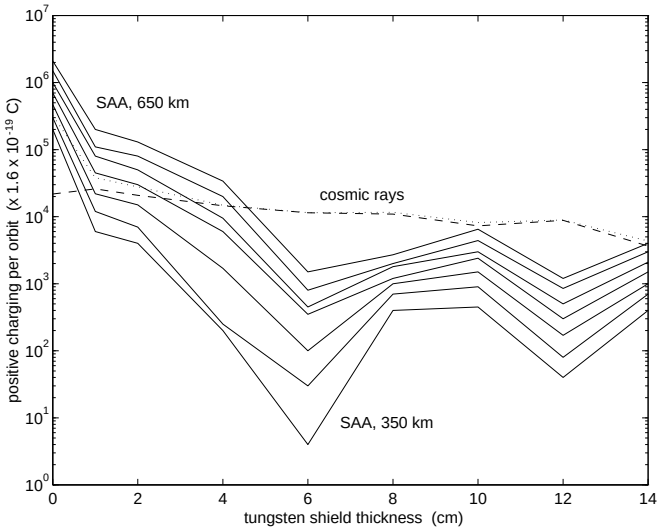

Figure 3. Computed charge (per orbit) of the STEP outer test mass due to the South Atlantic Anomaly (full curves, altitude steps of 50 km) and cosmic rays (broken curve). The dotted curve shows the sum (SAA plus cosmic rays) for the nominal STEP altitude of 400 km. All the results are for the solar minimum. At the solar maximum, the charging from the SAA is reduced by a factor of two, and, from cosmic rays, by a factor of four.

(which increases with thickness), and the distance they can travel (which decreases with distance). The minimum balance is achieved with approximately 6 cm of tungsten. The tungsten does little to suppress the effects of cosmic rays, even with 14 cm. This is because the cosmic rays have significant fluxes at energies up to 1000 MeV, requiring in excess of 25 cm of tungsten for complete shielding (impractical for a space mission).

Although GP-B has not been explicitly modelled, the results for STEP can be extrapolated to a first approximation (since both missions involve a polar orbit and a similar spacecraft/cryostat structure). Thus, scaling down the value in figure 3 (for zero tungsten thickness) at 650 km by the mass ratio of 4:1 between the STEP test masses and the GP-B gyroscopes, yields an estimated charge rate of $+8 \times 10^{-14}$ C per pass through the SAA (at the solar maximum) for GP-B. Considering eight SAA passes per day, this amounts to $\sim 1.5 \times 10^{9}$ protons/year. The cosmic-ray charging is negligible by comparison.

For LISA, cosmic rays are the dominant species when the Sun is inactive. The computations (including both hydrogen and helium) yield steady charge rates of 12 protons/s for the solar minimum and 3 protons/s for the solar maximum, with errors of $\pm 30\%$ due to the uncertainties in the spectra (error bars in figure 2).

For all missions, an average solar flare leads to charging of about 5×10^{-12} C kg^{-1}, and an anomalously large flare leads to 5×10^{-9} C kg^{-1}. The time history of the charging is correlated with the history of the flare event, so the data can simply be ignored during flares (as long as a subsequent discharging procedure is employed). For GP-B, which will fly near the solar maximum, the average expected charge rate from solar flares will be about 6×10^{6} protons/year, about two orders of magnitude less than the SAA charging, and thus negligible by comparison.

For low-inclination Earth orbits, solar protons cannot penetrate the geomagnetic field, and do not present a problem.

3.2. Accuracy of simulations

It is difficult to assess the absolute accuracy of the GEANT simulations or the environmental models (the AP8 models may only be accurate to within a factor of two, especially at higher energies). With this in mind, and acknowledging the consistency of the results with previous GEANT computations and with analytically derived results [9, 4], it is concluded that the charge rates presented are accurate to within a factor of two.

4. Charge management

4.1. Limiting requirements and charge tolerances

The implications of charging will depend on the experiment design, and on the amplitude and frequency of the science signals to be observed. This is elaborated by the following examples.

4.1.1. STEP. Superconducting shielding protects the STEP (and GP-B) payloads from Lorentz force disturbances, so the dominant effect of charge (Q) is via Coulomb interactions. For a test body at a potential V_T which sits inside an enclosure of electrodes with applied potentials, V_i, and which has a free charge, Q, the total electrostatic energy of the system is

$$E = \frac{1}{2}\sum C_i (V_i - V_T)^2 + \frac{1}{2}\frac{Q^2}{C} + QV_T \tag{1}$$

where $C = \sum C_i$ is the total capacitance of the test body with respect to its surrounding electrodes. The electrostatic suspension and control system will usually ensure $\sum C_i V_i = 0$ [4] in which case $V_T = 0$ and the force acting in any particular direction, x, is then

$$F_x = -\frac{\partial E}{\partial x} = -\frac{1}{2}\sum \frac{\partial C_i}{\partial x} V_i^2 + \frac{Q^2}{2C^2}\frac{\partial C}{\partial x} - \frac{Q}{C}\sum V_i \frac{\partial C_i}{\partial x}. \tag{2}$$

The first term results from the suspension/control voltages, the second from the interaction between the free charge and the surrounding conducting surfaces (image charges) and the third from the interaction between the free charge and any applied potentials on the electrodes. In a perfectly symmetric system, such that $\frac{\partial C}{\partial x} = 0$, the second term would be zero. However, in practice, machining tolerances and simultaneous positioning requirements introduce sufficient asymmetries such that this term becomes significant enough to drive the charge constraint. In the case of STEP's cylindrical test bodies with magnetic pancake pick-up coils at each end the second term in equation (2) can be written as

$$F_Q = \frac{1}{2C^2}\frac{\partial C}{\partial x} Q^2 \tag{3}$$

$$\cong \frac{Q^2}{2C^2} 4\pi\epsilon_0 \left(r_o^2 - r_i^2\right)\frac{\delta x}{d^3} \tag{4}$$

where r_o and r_i are the outer and inner radii of the cylindrical test body, d is the gap between the test-body surface and the magnetic pick-up coil and δx is the miscentring distance from the 'electrostatic centre'.

The charge build-up in time can be modelled as a quasi-linear term, incorporating the mean charging rates from the SAA and from cosmic rays, and two additional terms which

correct for the fact that the SAA charge comes in discrete bursts and for the geomagnetic modulation of the cosmic-ray charging rate, i.e.

$$Q(t) \approx \left(\frac{\Delta Q_{SAA}}{T_0} + \dot{Q}_{CR} \right) t + \Delta Q_{SAA} S(t) + \frac{\dot{Q}_{CR}}{2} \cos 2\omega_0 t \tag{5}$$

where ΔQ_{SAA} is the mean charge deposit for each pass through the SAA (from figure 3), $\dot{Q}_{CR}$ is the mean charging rate due to cosmic rays, T_0 is the orbit period, ω_0 is the orbit angular frequency and $S(t)$ is a 'sawtooth' function which corrects for the discrete nature of the charge deposits in the SAA, once the main trend has been extracted [9]. The third term allows for the cosmic-ray modulation.

The underlying time dependency in equation (3) is thus quadratic, but with some additional time dependency from the fact that the charge deposit through the SAA comes in discrete bursts whilst the cosmic-ray charging rate is modulated by the geomagnetic latitude.

In order that the disturbances do not exceed the desired equivalence principle measurement sensitivity of 10^{-16} m s^{-2} with a 10 : 1 margin, it is required that

$$F_Q(\omega_{ep}) < 10^{-18} \text{ N} \tag{6}$$

where ω_{ep} is the angular frequency at which the EP measurement is done. Similarly, in order to ensure that the delicate mass-centring is not disturbed, introducing a differential force modulation through the Earth's gravity gradient, it is required that

$$F_Q(\sim \text{DC}) < 10^{-15} \text{ N}. \tag{7}$$

These requirements place limits on the allowable charge rates, as follows. The worse-case situation for the EP measurement constraint is when the spacecraft is non-rotating and the charge deposits from SAA passes are arriving at close to the signal frequency. With some typical instrument values for the relevant parameters (C = 10–100 pF, d = 2 mm, $\partial C/\partial x \sim 5$ pF m^{-1}, $\delta x = 1$ μm) the limiting charge beyond which equation (6) is violated is $\sim 10^{-13}$ C. The centre-of-mass constraint gives a somewhat higher limit of 2×10^{-11} C.

Comparing these limits with the charge rates in figure 3, it is clear that a system must be employed every few orbits to remove the charge. For the nominal altitude of 400 km, additional use of a 2 cm tungsten shield lengthens the amount of time from ~ 2 to ~ 30 orbits between successive charge removal operations.

During periods when the EP measurement is carried out by rotating the spacecraft at a suitable rate, to displace the signal frequency from the orbit frequency, both the orbit-frequency charge limit (6) and the mass-centring constraint (7) are relaxed. This lengthens further the allowable time between charge removals.

4.1.2. GP-B. The GP-B gyroscopes are contained within an electrically conducting housing incorporating three orthogonal pairs of electrodes on which the electrostatic suspension and control voltages are applied. If the gyroscope becomes charged then electrostatic forces will arise according to equation (3). Derivations of capacitance gradients for this geometry are given in [4]. Torque and acceleration considerations limit the allowable rotor charge to 10 pC ($\equiv$ 10 mV potential on the 1 nF rotor capacitance). By contrast, the earlier charging rate estimate gives an accumulated charge over the 1.5 year mission of about 600 pC, making it necessary to monitor the gyroscope potential and use active charge control.

4.1.3. LISA. For LISA, the dominant disturbance is acceleration noise, a_n, arising from the Lorentz force interaction of any free charge on the test body with the interplanetary magnetic field, $\vec{B}$, through which the spacecraft is moving. The instantaneous force acting on the test body is

$$F = \frac{Q}{m}\vec{v} \wedge \vec{B} \tag{8}$$

where m is the test-body mass and $\vec{v}$ the spacecraft velocity. As a direct force this induces a drift of the test body which in itself is negligibly small [2]. However, fluctuations in the magnetic field and in the charge arrival rate will give rise to acceleration noise

$$a_n = \frac{1}{m}\delta Q\vec{v} \wedge \vec{B} + \frac{1}{m}\dot{\bar{Q}}t\vec{v} \wedge \delta\vec{B}. \tag{9}$$

The second term is by far the most dominant and using the spectral noise densities of Tu and Marsh [15] gives a charge limit of 1.3×10^{-13} C before a_n exceeds its budget figure of 2.5×10^{-16} m s^{-2} Hz$^{-1/2}$. With the charging rate of 12 protons/s established earlier this gives some seven days between charge removals. This can be improved by providing some level of electromagnetic shielding against Lorentz disturbances. This could either be through the use of a partially closed high permeability magnetic shielding or by simply ensuring a completely closed electrically conducting enclosure, in which case the Lorentz force induces a charge separation in the enclosure, which produces an internal field, which exactly cancels the Lorentz force 'seen' by the test body [3]. However, the gain by doing this is limited to a factor of 10 at which point the third term in equation (2) (the interaction of any free charge with any applied potentials) becomes the driving perturbation.

By contrast, the imparted *momentum* fluctuations from cosmic rays amount to $\sim 2 \times 10^{-18}$ m s^{-2} Hz$^{-1/2}$ (for the 1.2 kg mass), which is four orders of magnitude below the desired LISA sensitivity, and can thus be neglected. However, these momentum considerations will impose a practical limit for future advanced missions which attempt to achieve even higher sensitivities.

4.2. Charge measurement

In all three example missions the charge is measured using a force modulation technique [14], in which sinusoidal 'dither' voltages are applied 180° out of phase to two electrodes on opposite sides of the test body. If the test body is charged, this will induce an oscillatory motion of the test body.

For STEP and LISA this motion can be measured through the sensitive science signal channel. The choice of dither frequency is a compromise between measurement response time and system sensitivity. In STEP a frequency of 0.01 Hz is chosen and a voltage of ~ 0.2 V is needed to give a charge sensitivity sufficient to induce a (differential) motion which can be seen above the drag-free residual noise. A LISA dither frequency of 10 Hz, outside the science frequency range, using a 1 V drive voltage gives a sufficiently sensitive measurement within 100 s.

For GP-B the force modulation is measured from the suspension system feedback response. The dither frequency is about 1% of the feedback system bandwidth, ensuring that no actual motion of the gyroscope takes place. This technique achieves an accuracy of better than 4 mV for an integration time of 100 s, making it suitable for use with the GP-B mission. The method is insensitive to gyroscope miscentring and independent of the ambient acceleration.

4.3. The photoemission technique for charge removal

UV photoemission is the method used by GP-B to generate the electrons used for charge control. The rotor and biasing electrode are illuminated with UV light, and the electrons generated by photoemission from both these surfaces are added or removed from the rotor using a dedicated biasing electrode. The direction of the charge flow is controlled by biasing of the charge control electrode to ± 3 V with respect to the gyroscope surface. The gyroscope surface is a sputtered thin film of niobium, while the charge control electrode surface is electroplated with gold. Experimental considerations pose additional constraints on the hardware near the gyroscope: low remnant magnetization, very high standards of cleanliness, a superconducting transition temperature below 1.5 K and compatibility with the 2 K GP-B experimental temperature. Figure 4 shows results of the ground testing of the charge management system, which indicate that it meets GP-B requirements [4]. Note that the 1 g environment is much noisier and poses significantly more stringent requirements on the charge control system than the 10^{-7} g flight environment. In principle the GP-B technique can be adapted straightforwardly for STEP and GP-B although their much lower charge tolerances (and hence test-body potential limits) make the charge transfer requirements that much more delicate to match. This has implications for the stability of surface patch charge potentials and work function variations. Laboratory tests have shown that delivery of sufficient numbers of UV photons through fibre-optic systems is not a problem, but actual charge control on suspended electrically isolated test bodies at the levels of sensitivity required for both STEP and LISA remains to be demonstrated.

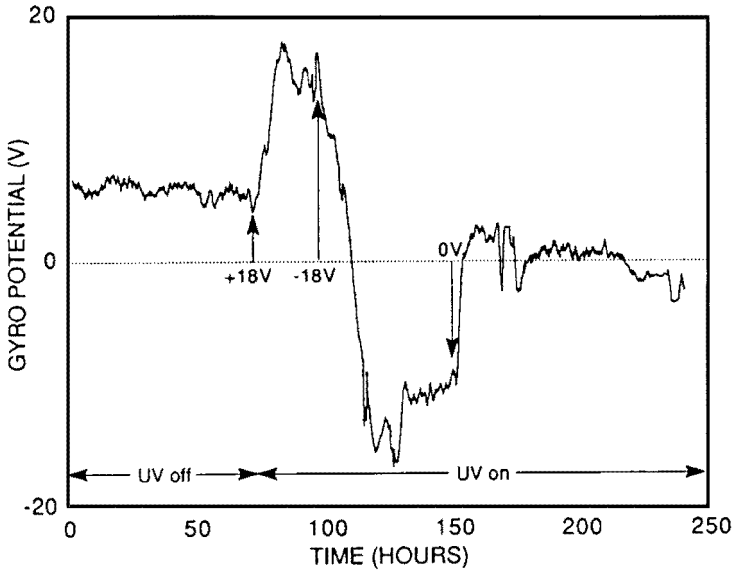

Figure 4. UV charge management test.

5. Conclusions

Monte Carlo computations confirm that electrostatic charging represents an important disturbance for precision space experiments. For Earth-orbiting spacecraft, the trapped particles and solar protons can be avoided with low-altitude (< 500 km), near-equatorial

orbits. Otherwise, shielding can be used to suppress the effects from trapped particles and solar flares down to the level of the (unshieldable) cosmic rays. Thereafter, the residual charge must be measured and removed using a method such as the photoemission technique discussed and already developed for the GP-B mission. Electromagnetic shielding should be used to reduce Lorentz forces, if possible, thus easing the requirements of the charge removal system.

Acknowledgments

YJ is grateful to P Nieminen (formerly at ESTEC, presently at the University of Bern) for setting up the revised GEANT models for STEP and LISA, and to F Camermans (ESTEC) for performing the low-energy electron calculations with ITS.

References

[1] Buchman S *et al* 1996 *Class. Quantum Grav.* **13** A185–91
[2] Bender P *et al* 1996 *LISA Pre-Phase A Report* MPQ 208
[3] Blaser J-P 1996 Private communication
[4] Buchman S, Quinn T, Keiser G M, Gill D and Sumner T J 1995 *Rev. Sci. Instrum.* **66** 120
[5] Brun R, Bruyant F, Maire M, McPherson A C and Zanarini P 1984 *GEANT3 User's Guide* DD/EE/84-1, CERN
[6] Danzmann K 1996 *Class. Quantum Grav.* **13** A247–50
[7] Feynman J *et al* 1993 *J. Geo. Res.* **98** 13 281
[8] Halbleib J A, Kensek R P, Mehlhorn T A, Valdez G D, Seltzer S M and Berger M J 1992 *ITS version 3.0: the Integrated TIGER Series of Coupled Electron/Photon Monte Carlo Transport Codes* SAND91–1634 UC–405, Sandia National Laboratories
[9] Jafry Y and Tranquille C 1995 An assessment of the charged particle environment during the STEP mission, and consequences for the payload *Proc. STEP Symp. (Pisa, 1993)*
[10] Jursa A S (ed) 1985 Handbook of geophysics and the space environment *Document no ADA 167000* United States Air Force Geophysics Laboratory
[11] King J H 1974 Solar proton fluences for 1977–1983 space missions *J. Spacecraft* **11** 401
[12] Lockerbie N A 1996 *Class. Quantum Grav.* **13** A53–7
[13] Sawyer D M and Vette J I 1976 AP8 trapped proton environment for solar maximum and solar minimum NSSDC 76-06, NASA-GSFC
[14] Sumner T J and Touboul P 1995 Charge management for STEP *Proc. STEP Symp. (Pisa, 1993)*
[15] Tu C-Y and Marsch E 1995 *Space Sci. Rev.* **73** 1–210
[16] Turneaure J P *et al* 1989 *Adv. Space Res.* **9** 29
[17] Vette J I 1991 The NASA/national space science data center trapped radiation environment model program (1964–1991) NSSDC/WDC-A-R&S 91-29